THE JOURNAL OF PHYSICAL CHEMISTRY C

Article

Cite This: J. Phys. Chem. C 2018, 122, 27582−27589

pubs.acs.org/JPCC

Developing ReaxFF to Visit CO Adsorption and Dissociation on Iron Surfaces

Kuan Lu,[†,‡,§] Yurong He,[†,‡,§] Chun-Fang Huo,*[,‡] Wen-Ping Guo,[‡] Qing Peng,*[,∥] Yong Yang,[†,‡] Yong-Wang Li,[†,‡] and Xiao-Dong Wen*[,†,‡]

[†]State Key Laboratory of Coal Conversion, Institute of Coal Chemistry, Chinese Academy of Sciences, Taiyuan, Shanxi 030001, P. R. China

[‡]National Energy Center for Coal to Clean Fuels, Synfuels China Co., Ltd., Huairou District, Beijing 101400, P. R. China

[§]University of Chinese Academy of Sciences, No. 19A Yuquan Road, Beijing 100049, P. R. China

[∥]Nuclear Engineering and Radiological Sciences, University of Michigan, Ann Arbor, Michigan 48109, United States

Supporting Information

ABSTRACT: We parameterize the ReaxFF potential, namely, RPOFeCO-2018, with substantial trainsets from first-principles calculations for modeling the chemical reactions in Fe/C/O systems using molecular dynamics simulations. We validate the new potential with the adsorption and dissociation of CO and C−C coupling, which has also considered the lateral interaction between adsorbed molecules. Using the new potential, we explored the structure−activity relationship between different iron surfaces and the adsorption or dissociation of CO. We find that the Fe(110) surface is inert for CO activation at the initial stage but keeps the high activity to CO dissociation in the long run compared with other surfaces including Fe(310) surface. Our results suggest the widely promising applications of the newly developed RPOFeCO-2018 reactive potential.

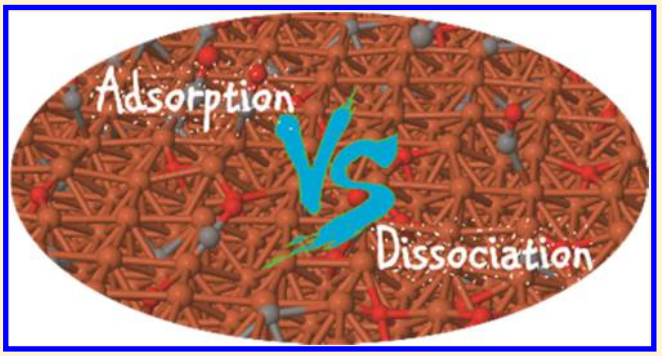

1. INTRODUCTION

CO adsorption on the different surfaces of iron, including low-index surface[1−4] and high-index surface,[5−8] from the theoretical and experimental methods has been extensively investigated because of its critical role in many industry catalytic processes, such as gasoline and diesel oil from the Fischer−Tropsch synthesis (F−T),[9] hydrogen gas from the water−gas shift,[10] metallic iron made by the blast furnace process,[11] and so on. For Fischer−Tropsch synthesis, iron carbides, such as Fe_5C_2[12−14] and Fe_3C[12−14] (relating to Fe−C interaction), are usually considered as the active phase whose formation suffers several process from the reduction to the carbonization of iron oxide under CO[15] (relation to Fe−C−O interaction) or syngas.[16] Furthermore, the products approximately object to the Anderson−Schulz−Flory distribution.[17] For water−gas shift, the redox mechanism[10] is thought to be dominant at the high temperature, which relates to the oxidation of $Fe^{2+} \rightarrow Fe^{3+}$ by H_2O and the reduction of $Fe^{3+} \rightarrow Fe^{2+}$ by CO (relation to Fe−C−O interaction). For better understanding and improving these industry catalytic processes, the accurate interatomic interactions between iron, carbon, and oxygen play a pivotal role in theoretical modeling of these chemicals.

The exploration of the above reaction mechanisms and how the catalyst affects the reaction process is still a grand challenge. There are a few experimental technologies including in situ X-ray absorption fine structure spectroscopy[14] and in situ X-ray diffraction[14] for this task. However, most of them are used to characterize the transformation of structure, resulting in lack of equipment to investigate the reaction process. Therefore, the relationships between the microstructure and the properties of iron and iron carbides are still obscure on the basis of the available experimental evidences. The development of reactive force field (ReaxFF) by van duin[18] in 2001 gives us new hope to explore the reaction processes because it is capable of comprehensively modeling the formation and breaking of chemical bonds within the framework of molecular dynamics simulations, which otherwise only possible in computing demands quantum mechanics methods. Furthermore, it can simultaneously model the physical and chemical interactions,[19] which commonly occur in the real reaction conditions.[20] In 2012, Zou et al.[21] developed the Fe/C/H potential to study the adsorption and dissociation of hydrogen on iron and iron carbides by merging the Fe/O/H potential[22] and reparameterizing the Fe−C−H interactions. After that, the valence angle formulation[23] with regard to the CHO molecule had been modified to make the C/H/O force field more suitable toward

Received: October 26, 2018
Revised: November 5, 2018
Published: November 8, 2018

DOI: 10.1021/acs.jpcc.8b10427
J. Phys. Chem. C 2018, 122, 27582−27589

the syngas combustion and initial oxidation kinetics. Though the CO oxidation had also been considered in their study, the effect of catalyst on the CO oxidation is still required. An accurate ReaxFF potential for the Fe/C/O system is desirable but lacking. On the basis of our previous work of reparameterizing the Fe−C ReaxFF potential,[24] we expanded the trainsets by including the Fe−C−O interactions to develop the Fe/C/O potential.

In this article, we first developed the Fe/C/O potential, named ReaxFF parameters of Fe/C/O (RPOFeCO-2018), and then validated its practicality. At last, we used the Fe/C/O potential to explore the adsorption and dissociation of CO on different iron surfaces to present its active difference. The rest of the article is organized as follows. The computational methods with details of first-principles calculations and ReaxFF methods are introduced in Section 2. The validation of the RPOFeCO-2018 potential is in Section 3, followed by the predictions in Section 4, and applications in Section 5. Finally, the conclusions are in Section 6.

2. COMPUTATIONAL METHODS

2.1. First-Principles Calculations. All first-principles data included in the trainset were obtained using the density functional theory (DFT) method implemented in the Vienna Ab initio simulation package (VASP).[25,26] The projector-augmented-wave method proposed by Blöchl[27] was used, which is an all-electron DFT technique to present the electron−ion interactions. The electron-exchange correlation was treated by the generalized gradient approximation in Perdew−Burke−Ernzerhof form,[28] as it can give a more accurate description of iron properties than ultrasoft pseudopotentials.[29] For the sake of accurate description of the magnetic properties of iron, the spin-polarized DFT calculations were carried out, which is also essential to the adsorption energy calculation. To ensure the energy errors are within the reasonable extent, an energy cutoff of 400 eV and the second-order Methfessel−Paxton[30] electron smearing with σ = 0.1 eV were used. The nudged elastic band[31] was exploited to locate the CO dissociation transition states on iron surfaces.

2.2. ReaxFF Method. ReaxFF is an empirical force field based on the concept of bond order.[18] ReaxFF is the function of bond length and bond energy, and it allows bond breakage and formation in a dynamic simulation. For the general form[24] of ReaxFF energy, one can refer to ref 24. One of the most important features of ReaxFF is the use of electronegativity equilibration method[32] with shielding to calculate the charge distribution. For every step, the charge distribution is updated. With additional energy terms, the charge distribution affects the geometry of atomistic structures and further affects the total potential energy of the materials. The bond orders calculation also updates every iteration, which firmly establishes the bonded interaction and the nonbonded interactions. The parameters (RPOFeCO-2018) were fitted to data from first-principle calculations. The fitting procedure uses genetic algorithm implemented in our home-made code.[24]

The reactive molecular dynamics (RMD) simulations were performed using the large-scale atomic/molecular massively parallel simulator[33] adopting a time step of 0.00025 ps. The Berendsen thermostat[34] was used to control the temperature with a damping constant of 0.1 ps. Energy minimized via a conjugate gradient or a nonreaction relaxation was conducted before each RMD simulation. The trajectories were dumped every 0.1 ps.

3. VALIDATION OF FE/C/O POTENTIAL

On the basis of our previous work about Fe−C interaction trainset,[24] additional extensive VASP calculation were performed to build a comprehensive Fe/C/O interaction training set, including the CO stepwise adsorption energy on the Fe(100) surface and a serial reaction process consisting of the CO dissociation and C−C coupling on the iron carbides. Then, the trainset was used to develop the parameters for the Fe/C/O interaction. The new Fe/C/O potential are shown in the Supporting Information.

3.1. Adsorption of *n*CO. The adsorption of CO on the surface is the first step to activate and continue the following reactions. To model the real adsorption environments, we considered the lateral interaction between molecules by total adsorption of multiple CO on the Fe(100) surface. The total adsorption energy (TAE), $\Delta E_{TAE} = E_{n(CO)/slab} - [E_{slab} + nE_{CO}]$, was used to evaluate the overall ability of the new potential compared with the VASP results, where $E_{n(CO)/slab}$ is the total energy of the slab with nCO adsorption, E_{slab} is the energy of clean slab, and E_{CO} is the energy of a free CO molecule in the gas phase. The lower the difference between ReaxFF and VASP results, the better the performance of the new potential is. The difference between $(n + 1)$CO adsorption and nCO adsorption donates the stepwise adsorption energy, defined by $\Delta E_{ads} = E_{(n+1)CO/slab} - [E_{n(CO)/slab} + E_{CO}]$. The most stable sites of CO adsorption one by one were screened from the abounding attempt of CO adsorption on the different iron surfaces.[2,6]

The total adsorption energy of CO in a few molecules region calculated by RPOFeCO-2018 potential (Figure 1) is well

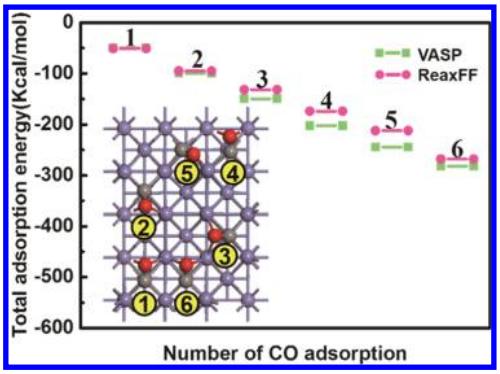

Figure 1. The total adsorption energy (TAE) of CO on the Fe(100) surface. The inset graph shows the order of CO adsorption and its corresponding adsorption sites. Color scheme: iron atom (blue), carbon atom (black), and oxygen atom (red). The same color scheme is applied to the following figures.

consistent with the VASP data and reference data.[2] When the adsorbed CO numbers exceeds two, the total adsorption energy of CO gradually deviates from the VASP data. The stepwise adsorption energy calculated by RPOFeCO-2018 is also comparable with the VASP data. The overall trend of our ReaxFF results is analogous to that of VASP, indicating that the RPOFeCO-2018 can correctly describe the CO adsorption when CO numbers are small, as well as the effect of lateral interaction when the CO numbers are large.

3.2. Dissociation of CO on Fe_xC_y. Owing to the vacancy formed by the escape of surface carbon from Fe_xC_y, the CO dissociation barrier can decrease largely compared with the perfect Fe_xC_y surfaces.[13] Apart from the CO dissociation on the perfect $Fe_5C_2(010)$ and $Fe_3C(001)$ surface, we considered the

DOI: 10.1021/acs.jpcc.8b10427
J. Phys. Chem. C 2018, 122, 27582−27589

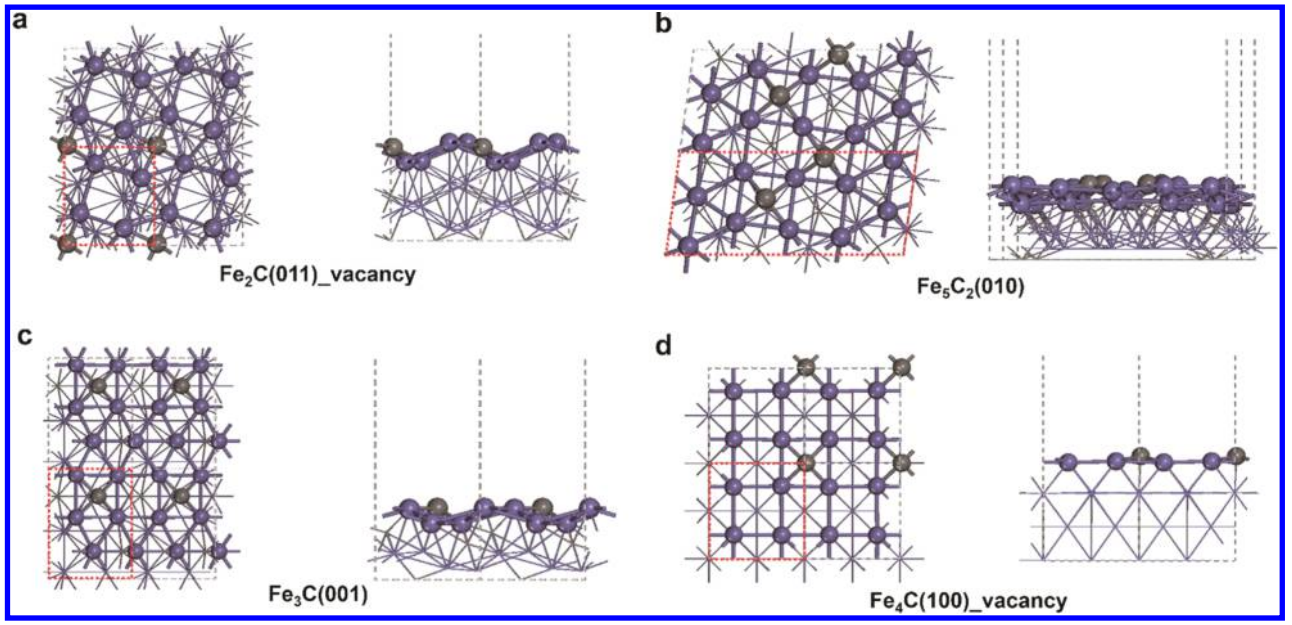

Figure 2. Top and side views of the Fe_xC_y surfaces. (a) Fe_2C (011): $p(1 \times 1)$. (b) $Fe_5C_2(010)$: $p(1 \times 1)$. (c) $Fe_3C(001)$: $p(1 \times 1)$. (d) $Fe_4C(100)$: $p(\sqrt{2} \times \sqrt{2})$. The color scheme is the same as in Figure 1.

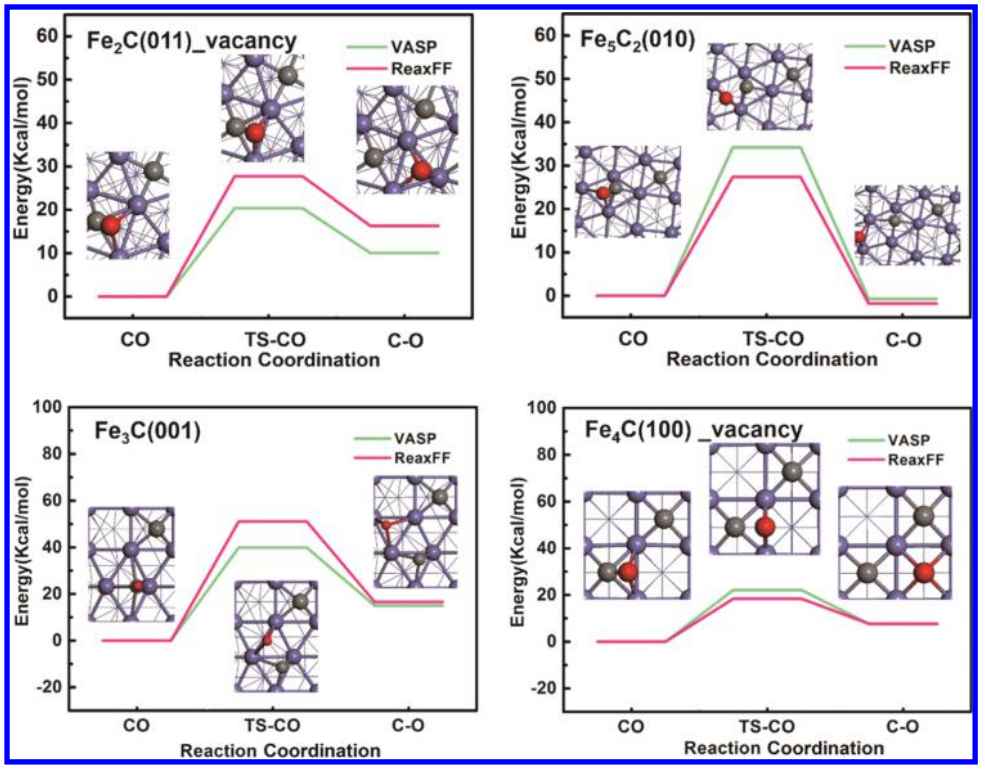

Figure 3. The CO dissociation and its corresponding structures of initial state, transition state (TS), and final state on Fe_xC_y. The color scheme is the same as in Figure 1.

effect of vacancy on the CO dissociation by constructing vacant $Fe_2C(011)$ and $Fe_4C(100)$ surface (Figure 2). The reaction energy and barrier were calculated by $\Delta_r E = E_{FS} - E_{IS}$ and $E_a = E_{TS} - E_{IS}$, where E_{IS}, E_{FS}, and E_{TS} are the energies of the corresponding initial state (IS), final state (FS), and transition state (TS), respectively. Figure 3 shows that the CO dissociation barrier agrees excellently with the results of VASP and the reference value.[13] The error bar of about 8 kcal/mol by RPOFeCO-2018 is acceptable,[35−37] implying that the RPOFeCO-2018 potential can well describe the CO dissociation not only on perfect Fe_xC_y surfaces but also on the defected surfaces.

3.3. C−C Coupling and Hydrogenation of CO. It is generally believed that the hydrogenation process is after the CO and H_2 dissociation. The C−C coupling and the CH_x hydrogenation are the key steps for F−T synthesis. When iron carbides are exposed to the syngas (CO/H_2), a competition occurs between the hydronation of the adsorbed CO and its coupling with the surface C atom ($C_{(s)}$). As shown in Figure 4,

DOI: 10.1021/acs.jpcc.8b10427
J. Phys. Chem. C 2018, 122, 27582−27589

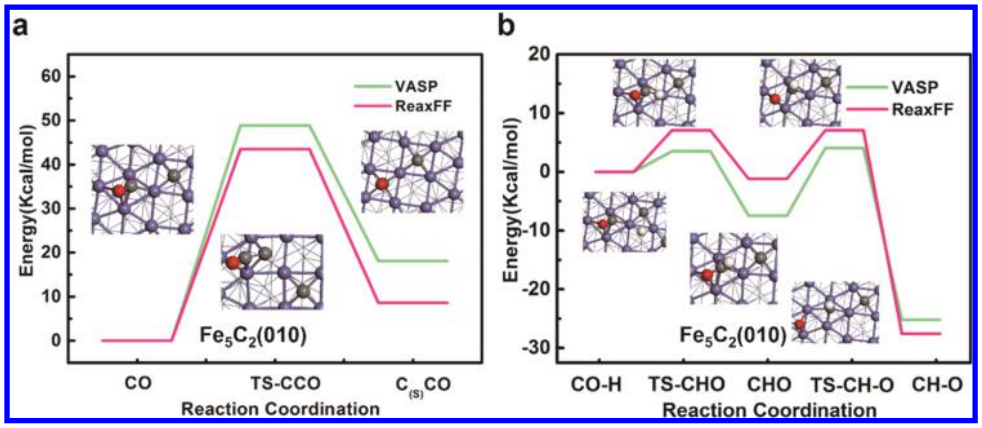

Figure 4. (a) C−C coupling process. (b) Hydrogenation process of CO to CH. Color scheme: iron atom (blue), carbon atom (black), oxygen atom (red), and hydrogen (white).

the barrier of CO hydrogenation (Figure 4b) is lower than the C−C coupling (Figure 4a) on $Fe_5C_2(010)$ surface. Also, the existence of H element on the $Fe_5C_2(010)$ surface make the CO dissociation barrier lower than the direct CO dissociation (Figure 3). This result indicates that the RPOFeCO-2018 can describe such a competition. In addition, RPOFeCO-2018 can regenerate the thermal stability between the adsorption species. Our results are consistent with a previous investigation.[13] It is worth mentioning that this study focuses on the optimization of Fe−C−O interactions only. The reparameterizing of Fe−C−O−H interactions are among the list of our future tasks.

4. PREDICTIONS

To further validate the new potential, we have examined some structures from the thermodynamics and dynamic aspects. All these structures are part of the total trainset, but it is only to validate our potential. It dose not take part in the fitting process. Figure 5 shows the total adsorption energy and stepwise

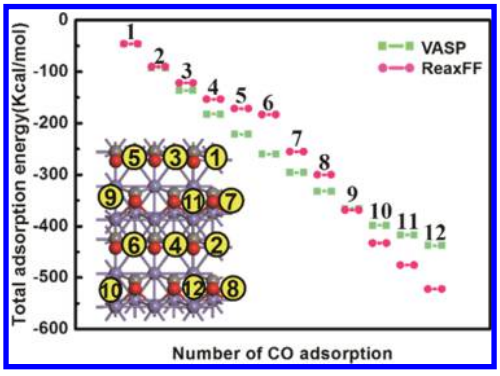

Figure 5. The total adsorption energy of CO on the Fe(210) surface. The inset graph shows the order of CO adsorption and its corresponding adsorption sites. The color scheme is the same as in Figure 1.

adsorption of 12 CO on the Fe(210) surface. We can see that the RPOFeCO-2018 can well reproduce the adsorption behavior when the CO coverage is lower. When the coverage reaches saturation, a perceptible deviation is observed. However, such a discrepancy might be negligible because in the experimental conditions, adsorption and dissociation are dynamic processes and saturation is hard to reach in a shorter time.[38] Therefore, the RPOFeCO-2018 can roughly present the CO adsorption trend on the different iron surfaces.

In addition, the RPOFeCO-2018 can regenerate the CO dissociation process when single CO is on the Fe(110) surface, as shown in Figure 6a. When the Fe(110) surface with a CO middle is moderately covered (Figure 6b), the RPOFeCO-2018 correctly describes the effect of lateral interaction compared with the results of Figure 6a. CO dissociation is relatively difficult at high coverage. Our results manifest that the RPOFeCO-2018 can well display the dynamic behavior of CO on the iron different surfaces.

5. APPLICATIONS: COMPETITION BETWEEN ADSORPTION AND DISSOCIATION OF CO ON DIFFERENT α-FE SURFACES

To investigate the structure−activity relationship between the surfaces' structure and the CO activation in the carburization of iron while giving results a statistical meaning, we conducted three parallel simulations for every single RMD simulation close to real conditions. Every single RMD simulation in three parallel simulations had its dependent initial velocity, and the single RMD simulation for different surfaces (Figure 7a) was performed with 50 CO molecules in the gas phase (Figure 7b) in the canonical (NVT) ensemble. All the molecules were placed uniformly above the surface about 0.5 nm. We used the large enough three-dimensional periodic systems: 10 × 10 × 12 with top 8 layers relaxed and bottom 4 layers fixed for Fe(110), 9 × 6 × 18 with top 12 layers relaxed and bottom 6 layers fixed for Fe(211), 8 × 5 × 24 with top 18 layers relaxed and bottom 6 layers fixed for Fe(310), 8 × 8 × 16 with top 10 layers relaxed and bottom 6 layers fixed for Fe(100), and 6 × 6 × 27 with top 18 layers relaxed and bottom 9 layers fixed for Fe(111), respectively. The reaction temperature was 500 K. The maximum simulation time was 250 ps. The average results of three parallel simulations are shown in Figure 8 and 9.

Single CO dissociation on the Fe(100) surface have been observed by the "lying down" precursor state, which is consistent with the experimental observation.[39] All the surfaces have the competition between CO dissociation and adsorption, which is also in agreement with the experimental phenomenon.[40−43] Figure 8a presents the conversion rate of CO on different surfaces in the order of (110) > (100) > (211) > (111) > (310), where the conversion rate of CO on the Fe(110) surface reached 76%. The CO conversion rate is defined as the difference between the initial and the final CO numbers in vacuum. As the reaction proceeds, the ability of different surfaces to dissociate CO changes greatly (Figure 8b). Here, the CO dissociation

DOI: 10.1021/acs.jpcc.8b10427
J. Phys. Chem. C 2018, 122, 27582−27589

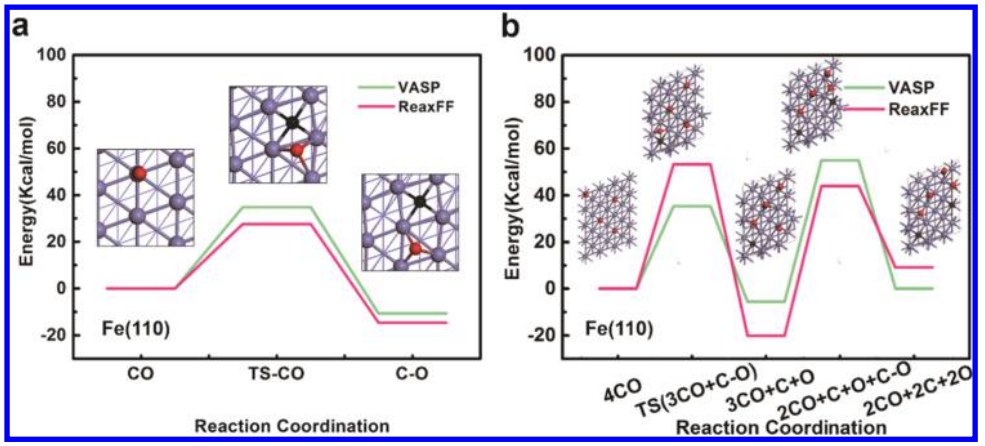

Figure 6. Dissociation of CO on the Fe(110) surface. (a) Single CO dissociation. (b) CO stepwise dissociation. The color scheme is the same as in Figure 1.

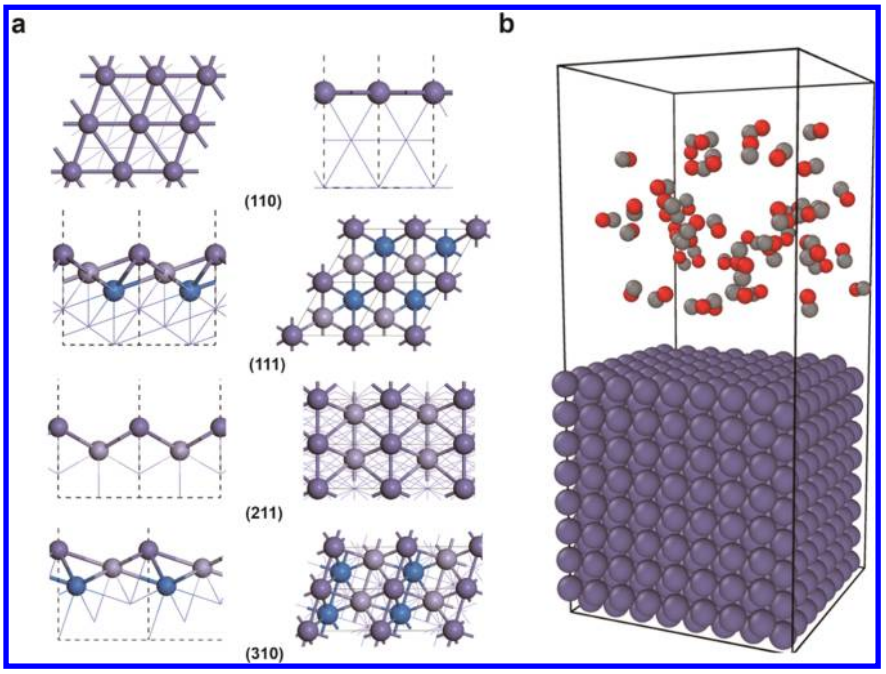

Figure 7. (a) Different surfaces structure of α-Fe. (b) Initial structure of CO adsorption and dissociation model on the Fe(100) surface.

ability is roughly expressed by the number of CO dissociation on the iron surface. For different surfaces, the order of initial CO dissociation ability is (310) ≈ (100) ≈ (111) ≈ (211) > (110). Our results agree well with a previous investigation,[6] where the Fe(110) surface had the highest barrier for single CO dissociation and other surfaces had close but relatively lower barrier values. At time of 10 ps, the CO dissociation rate of the Fe(310) surface drops sharply, the order of CO dissociation number for different surface changed to (100) > (211) > (111) > (110) > (310). In the overall process, the CO dissociation number of the Fe(110) surface steadily increases. At 25 ps, its dissociation number is equal to that of other surfaces, and the number reaches the maximum at 60 ps and remains constant thereafter. Owing to the existence of the inactive phenomenon for other surfaces, the CO dissociation number changed to (110) > (100) > (211) > (111) > (310).

There are two reasons for the Fe(110) surface to remain active. First, the competition between dissociation and adsorption of CO becomes strong for the Fe(110) surface (Figure 8d). Owing to the high coordination number, the behavior of CO on this surface is dominated by adsorption state in the initial stage. As the reaction proceeds, the behavior of CO gradually turns to be dominated by the dissociation state. The similar behavior also exists in the Fe(211) surface. Other surfaces have the opposite trend. The higher-surface-energy surfaces, such as Fe(310), are quickly stabilized, resulting in a relatively slower dissociation rate for subsequent CO, consistent with a previous study.[6] For the Fe(110) surface, the surface energy reduction is a relatively time-consuming process because of its higher stability; therefore, it can provide the long-term driving force.

The other reason is that the Fe(110) surface has the strongest carbon penetration ability (Figure 9). We have added randomly 0.50 monolayer (ML), 0.75 ML, and 1.00 ML carbon atoms to different iron surfaces based on clean surface models, respectively. We assume that all the surfaces have the same ability to provide carbon atoms. One ML means the ratio of the added surface carbon atoms to the surface iron atoms is one. The maximum simulation time is 1 ns. The number of penetrated carbon atoms are counted when the carbons penetrate into the

DOI: 10.1021/acs.jpcc.8b10427
J. Phys. Chem. C 2018, 122, 27582−27589

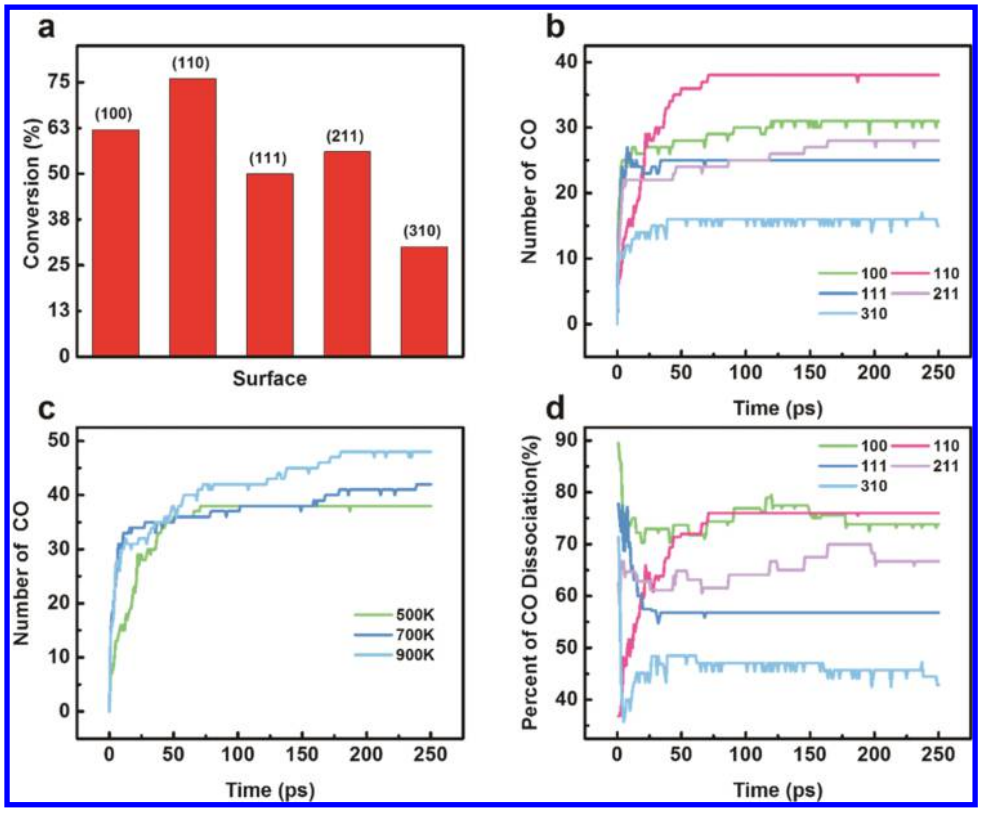

Figure 8. (a) Conversion rate of CO on five different iron surfaces. (b) Numbers of CO dissociation on five different iron surfaces. (c) Numbers of CO dissociation on the Fe(110) surface under different temperatures. (d) Competition between adsorption and dissociation of CO on five different iron surfaces.

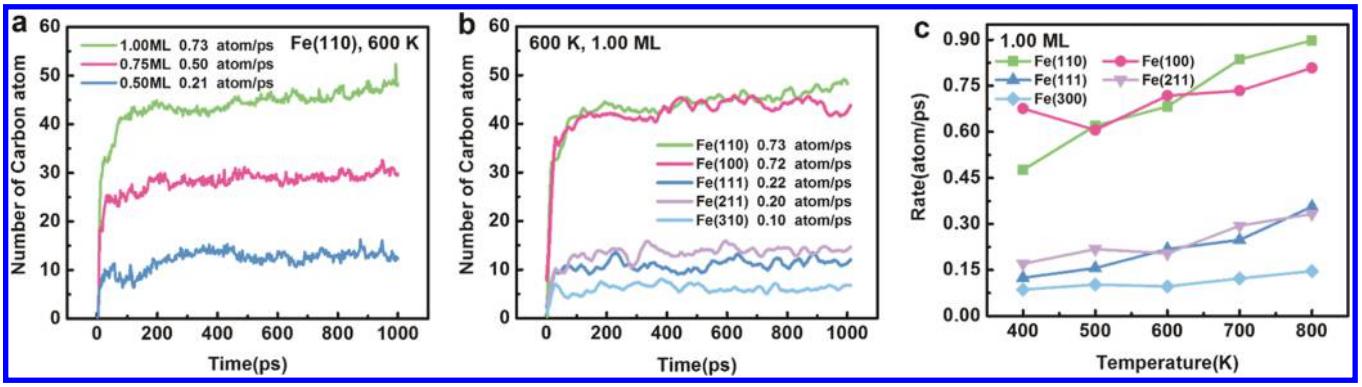

Figure 9. (a) Carbon penetration process for the Fe(110) surface at different carbon coverages (b) Carbon penetration process for different iron surfaces at 600 K and 1 monolayer (ML). The value of carbon penetration rate is the value at the 50 ps. The same scheme is used in (c). (c) Carbon penetration rate for different surfaces at different temperatures and 1 ML.

iron subsurface. Figure 9b,c shows that the Fe(110) and Fe(100) surfaces have the largest carbon penetration rate, which means that these surfaces can release quickly the surface active sites for the subsequent CO dissociation. At low coverages, the Fe(110) surface has a lower carbon penetration rate (Figure 9a). Accordingly, we can infer that other surfaces may also have a lower carbon penetration rate. As shown in Figure 9c, the penetration ability of Fe(111), Fe(211), and Fe(310) is relative weak at temperature range from 400 to 800 K, resulting in the surface being blocked by a lot of adsorbed carbon.

Temperature also has a positive effect on the CO dissociation. With the increasing temperature, the CO dissociation ability also increases (Figure 8c). In addition, the metal iron produced by the reduction of fresh iron-based catalyst under H_2 mainly composes the Fe(110) surface. Therefore, the Fe(110) surface is the surface that can maintain the CO activity for a long time under near real conditions at the pure CO atmosphere. Other surfaces are rapidly inactivated due to relatively rapid activation of CO or reconstruction.

6. CONCLUSIONS

We reparameterized Fe−C−O ReaxFF potentials with the extended training set with the addition of the first-principles data including the adsorption and dissociation processes of CO on Fe and Fe_xC_y, the carbon−carbon coupling on the Fe_5C_2 surface, and the CO hydrogenation on the surface of Fe_5C_2. We obtained the ReaxFF potential RPOFeCO-2018 with validation. We then used this potential function to explore the effect of different

DOI: 10.1021/acs.jpcc.8b10427
J. Phys. Chem. C 2018, 122, 27582−27589

surfaces of Fe on CO adsorption and dissociation. The results show that under near real conditions, CO activation on the Fe(110) surface is slower than that on other surfaces in the initial stage, but other surfaces inactivate rapidly due to their faster CO dissociation activity and slower carbon penetration rate. However, the most inert surface, the Fe(110) surface, can maintain long-term CO dissociation activity due to slower deactivation. Therefore, the Fe(110) surface is the major dissociation surface of CO under near real experimental conditions. Our results manifest that the RPOFeCO-2018 can regenerate the thermodynamics and dynamic behavior related to the interaction between Fe, C, and O and is suitable to describe the Fe/C/O interaction in the reaction process as close to real reaction conditions.

■ ASSOCIATED CONTENT

Supporting Information

The Supporting Information is available free of charge on the ACS Publications website at DOI: 10.1021/acs.jpcc.8b10427.

Potential for Fe−C−O interactions (TXT)

Additional data included in the ReaxFF trainset for RPOFeCO-2018 potential (PDF)

■ AUTHOR INFORMATION

Corresponding Authors

*E-mail: huochunfang@synfuelschina.com.cn (C.-F.H.).

*E-mail: qpeng@umich.edu (Q.P.).

*E-mail: wxd@sxicc.ac.cn (X.-D.W.).

ORCID

Xiao-Dong Wen: 0000-0001-5626-8581

Notes

The authors declare no competing financial interest.

■ ACKNOWLEDGMENTS

The authors are grateful for the financial support from the National Natural Science Foundation of China (Nos. 21473229, 91545121, 21603252, 21703274, 21703272, and 21273261), Shanxi Province Science Foundation for Youth (No. 201601D021048), Chinese Academy of Science and Synfuels CHINA. Co., Ltd. They also acknowledge the innovation foundation of the Institute of Coal Chemistry, Chinese Academy of Sciences, Hundred-Talent Program of Chinese Academy of Science, Shanxi Hundred-Talent Program, and National Thousand Young Talents Program of China.

■ REFERENCES

(1) Mehandru, S. P.; Anderson, A. B. Binding and Orientations of CO on Fe(110), (100), and (111): A Surface Structure Effect from Molecular Orbital Theory. *Surf. Sci.* **1988**, *201*, 345−360.

(2) Wang, T.; Tian, X.; Li, Y.-W.; Wang, J.; Beller, M.; Jiao, H. High Coverage CO Activation Mechanisms on Fe(100) from Computations. *J. Phys. Chem. C* **2014**, *118*, 1095−1101.

(3) Merrill, P. B.; Madix, R. J. Site Blocking by Hydrogen: CO on Clean and H-Presaturated Fe(100). *Surf. Sci.* **1992**, *271*, 81−84.

(4) Burke, M. L.; Madix, R. J. Effect of CO on Hydrogen Thermal Desorption from Fe(100). *Surf. Sci.* **1990**, *237*, 20−34.

(5) Elahifard, M. R.; Pérez Jigato, M.; Niemantsverdriet, J. W. Ab-Initio Calculations of the Direct and Hydrogen-Assisted Dissociation of CO on Fe(310). *Chem. Phys. Lett.* **2012**, *534*, 54−57.

(6) Wang, T.; Tian, X.-X.; Li, Y.-W.; Wang, J.; Beller, M.; Jiao, H. Coverage-Dependent CO Adsorption and Dissociation Mechanisms on Iron Surfaces from DFT Computations. *ACS Catal.* **2014**, *4*, 1991−2005.

(7) Jenkins, S. J. Dissociative Adsorption and Adsorbate-Induced Reconstruction on Fe(211). *Surf. Sci.* **2006**, *600*, 1431−1438.

(8) Borthwick, D.; Fiorin, V.; Jenkins, S. J.; King, D. A. Facile Dissociation of CO on Fe(211): Evidence from Microcalorimetry and First-Principles Theory. *Surf. Sci.* **2008**, *602*, 2325−2332.

(9) de Smit, E.; Weckhuysen, B. M. The Renaissance of Iron-Based Fischer-Tropsch Synthesis: On the Multifaceted Catalyst Deactivation Behaviour. *Chem. Soc. Rev.* **2008**, *37*, 2758−2781.

(10) Zhu, M.; Wachs, I. E. Iron-Based Catalysts for the High-Temperature Water−Gas Shift (HT-WGS) Reaction: A Review. *ACS Catal.* **2016**, *6*, 722−732.

(11) Geng, S.; Ding, W.; Guo, S.; Zou, X.; Zhang, Y.; Lu, X. Carbon Deposition on Iron Surfaces in CO−CO_2 Atmosphere. *Ironmaking Steelmaking* **2015**, *42*, 714−720.

(12) Le Caer, G.; Dubois, J. M.; Pijolat, M.; Perrichon, V.; Bussiere, P. Characterization by Moessbauer Spectroscopy of Iron Carbides Formed by Fischer-Tropsch Synthesis. *J. Phys. Chem.* **1982**, *86*, 4799−4808.

(13) Huo, C. F.; Li, Y. W.; Wang, J.; Jiao, H. Insight into CH_4 Formation in Iron-Catalyzed Fischer-Tropsch Synthesis. *J. Am. Chem. Soc.* **2009**, *131*, 14713−14721.

(14) de Smit, E.; Cinquini, F.; Beale, A. M.; Safonova, O. V.; van Beek, W.; Sautet, P.; Weckhuysen, B. M. Stability and Reactivity of η-χ-θ Iron Carbide Catalyst Phases in Fischer-Tropsch Synthesis: Controlling μC. *J. Am. Chem. Soc.* **2010**, *132*, 14928−14941.

(15) Wang, R.; Wu, B.; Li, Y. Synthesis of Single-Phase Iron Carbides and Their Adsorption Performance. *Chin. J. Catal.* **2012**, *33*, 863−869.

(16) Janbroers, S.; Crozier, P. A.; Zandbergen, H. W.; Kooyman, P. J. A Model Study on the Carburization Process of Iron-Based Fischer−Tropsch Catalysts Using in situ TEM−EELS. *Appl. Catal., B* **2011**, *102*, 521−527.

(17) Torres Galvis, H. M.; Bitter, J. H.; Davidian, T.; Ruitenbeek, M.; Dugulan, A. I.; de Jong, K. P. Iron Particle Size Effects for Direct Production of Lower Olefins from Synthesis Gas. *J. Am. Chem. Soc.* **2012**, *134*, 16207−16215.

(18) van Duin, A. C. T.; Dasgupta, S.; Lorant, F.; Goddard, W. A., III ReaxFF: A Reactive Force Field for Hydrocarbons. *J. Phys. Chem. A* **2001**, *105*, 9396−9409.

(19) Lu, K.; Huo, C.-F.; He, Y.; Yin, J.; Liu, J.; Peng, Q.; Guo, W.-P.; Yang, Y.; Li, Y.-W.; Wen, X. Grain Boundary Plays a Key Role in Carbon Diffusion in Carbon Irons Revealed by a ReaxFF Study. *J. Phys. Chem. C* **2018**, *122*, 23191−23199.

(20) Mao, J.; Chen, W.; Sun, W.; Chen, Z.; Pei, J.; He, D.; Lv, C.; Wang, D.; Li, Y. Rational Control of the Selectivity of a Ruthenium Catalyst for Hydrogenation of 4-Nitrostyrene by Strain Regulation. *Angew. Chem., Int. Ed.* **2017**, *56*, 11971−11975.

(21) Zou, C.; van Duin, A. C. T.; Sorescu, D. C. Theoretical Investigation of Hydrogen Adsorption and Dissociation on Iron and Iron Carbide Surfaces Using the ReaxFF Reactive Force Field Method. *Top. Catal.* **2012**, *55*, 391−401.

(22) Aryanpour, M.; van Duin, A. C. T.; Kubicki, J. D. Development of a Reactive Force Field for Iron-Oxyhydroxide Systems. *J. Phys. Chem. A* **2010**, *114*, 6298−6307.

(23) Ashraf, C.; van Duin, A. C. Extension of the ReaxFF Combustion Force Field toward Syngas Combustion and Initial Oxidation Kinetics. *J. Phys. Chem. A* **2017**, *121*, 1051−1068.

(24) Lu, K.; Huo, C. F.; Guo, W. P.; Liu, X. W.; Zhou, Y.; Peng, Q.; Yang, Y.; Li, Y. W.; Wen, X. D. Development of a Reactive Force Field for the Fe-C Interaction to Investigate the Carburization of Iron. *Phys. Chem. Chem. Phys.* **2018**, *20*, 775−783.

(25) Kresse, G.; Furthmuller, J. Efficiency of Ab-Initio Total Energy Calculations for Metals and Semiconductors Using a Plane-Wave Basis Set. *Comput. Mater. Sci.* **1996**, *6*, 15−50.

(26) Kresse, G.; Furthmüller, J. Efficient Iterative Schemes for Ab Initio Total-Energy Calculations Using a Plane-Wave Basis Set. *Phys. Rev. B* **1996**, *54*, 11169−11186.

(27) Blöchl, P. E. Projector Augmented-Wave Method. *Phys. Rev. B* **1994**, *50*, 17953−17979.

DOI: 10.1021/acs.jpcc.8b10427
J. Phys. Chem. C 2018, 122, 27582−27589

(28) Perdew, J. P.; Burke, K.; Ernzerhof, M. Generalized Gradient Approximation Made Simple. *Phys. Rev. Lett.* **1996**, *77*, 3865−3868.
(29) Schwerdtfeger, P. The Pseudopotential Approximation in Electronic Structure Theory. *ChemPhysChem* **2011**, *12*, 3143−3155.
(30) Methfessel, M.; Paxton, A. T. High-Precision Sampling for Brillouin-Zone Integration in Metals. *Phys. Rev. B* **1989**, *40*, 3616−3621.
(31) Henkelman, G.; Jónsson, H. Improved Tangent Estimate in the Nudged Elastic Band Method for Finding Minimum Energy Paths and Saddle Points. *J. Chem. Phys.* **2000**, *113*, 9978−9985.
(32) Rappe, A. K.; Goddard, W. A., III Charge Equilibration for Molecular Dynamics Simulations. *J. Phys. Chem.* **1991**, *95*, 3358−3363.
(33) Plimpton, S. Fast Parallel Algorithms for Short-Range Molecular Dynamics. *J. Comput. Phys.* **1995**, *117*, 1−19.
(34) Berendsen, H. J. C.; Postma, J. P. M.; Van Gunsteren, W. F.; Dinola, A.; Haak, J. R. Molecular Dynamics with Coupling to an External Bath. *J. Chem. Phys.* **1984**, *81*, 3684−3690.
(35) Senftle, T. P.; Meyer, R. J.; Janik, M. J.; van Duin, A. C. T. Development of a ReaxFF Potential for PdO and Application to Palladium Oxide Formation. *J. Chem. Phys.* **2013**, *139*, No. 044109.
(36) Agrawalla, S.; van Duin, A. C. T. Development and Application of a ReaxFF Reactive Force Field for Hydrogen Combustion. *J. Phys. Chem. A* **2011**, *115*, 960−972.
(37) Mueller, J. E.; van Duin, A. C. T.; Goddard, W. A., III Development and Validation of ReaxFF Reactive Force Field for Hydrocarbon Chemistry Catalyzed by Nickel. *J. Phys. Chem. C* **2010**, *114*, 4939−4949.
(38) Nassir, M. H.; Frhberger, B.; Dwyer, D. J. Coverage Dependence of CO Dissociation on Clean and Hydrogen Presaturated Fe(100) Surface. *Surf. Sci.* **1994**, *312*, 115−123.
(39) Benndorf, C.; Krüger, B.; Thieme, F. Unusually Low Stretching Frequency for CO Adsorbed on Fe(100). *Surf. Sci. Lett.* **1985**, *163*, L675−L680.
(40) Yoshida, K.; Somorjai, G. A. The Chemisorption of CO, CO_2, C_2H_2, C_2H_4, H_2 and NH_3 on the Clean Fe(100) and (111) Crystal Surfaces. *Surf. Sci.* **1978**, *75*, 46−60.
(41) Moon, D. W.; Dwyer, D. J.; Bernasek, S. L. Adsorption of CO on the Clean and Sulfur Modified Fe(100) Surface. *Surf. Sci.* **1985**, *163*, 215−229.
(42) Seip, U.; Tsai, M. C.; Christmann, K.; Küppers, J.; Ertl, G. Interaction of CO with an Fe(111) Surface. *Surf. Sci.* **1984**, *139*, 29−42.
(43) Bartosch, C. E.; Whitman, L. J.; Ho, W. The Adsorption, Interconversion, and Dissociation of CO on Fe(111). *J. Chem. Phys.* **1986**, *85*, 1052−1060.

DOI: 10.1021/acs.jpcc.8b10427
J. Phys. Chem. C 2018, 122, 27582−27589